Cell-Permeable Ln(III) Chelate-Functionalized InP Quantum Dots As Multimodal Imaging Agents

Graeme J. Stasiuk,[†] Sudarsan Tamang,[‡] Daniel Imbert,[†] Cathy Poillot,[§] Marco Giardiello,[†] Céline Tisseyre,[§] Emmanuel L. Barbier,[§] Pascal Henry Fries,[†] Michel de Waard,[§] Peter Reiss,[‡] and Marinella Mazzanti[†,*]

[†]CEA-Grenoble, INAC, SCIB, Laboratoire de Reconnaissance Ionique et Chimie de Coordination, UMR-E 3 CEA-UJF, 38054 Grenoble Cedex 9, France, [‡]CEA Grenoble, INAC, SPrAM, Laboratoire d'Electronique Moléculaire, Organique et Hybride, UMR 5819 CEA-CNRS-UJF, France, and [§]Grenoble Institute of Neuroscience, Inserm U836, Site Santé de la Tronche, Bâtiment Edmond J. Safra, Chemin Fortuné Ferrini, BP170, 38042, France

ABSTRACT Quantum dots (QDs) are ideal scaffolds for the development of multimodal imaging agents, but their application in clinical diagnostics is limited by the toxicity of classical CdSe QDs. A new bimodal MRI/optical nanosized contrast agent with high gadolinium payload has been prepared through direct covalent attachment of up to 80 Gd(III) chelates on fluorescent nontoxic InP/ZnS QDs. It shows a high relaxivity of 900 mM^{-1} s^{-1} (13 mM^{-1} s^{-1} per Gd ion) at 35 MHz (0.81 T) and 298 K, while the bright luminescence of the QDs is preserved. Eu(III) and Tb(III) chelates were also successfully grafted to the InP/ZnS QDs. The absence of energy transfer between the QD and lanthanide emitting centers results in a multicolor system. Using this convenient direct grafting strategy additional targeting ligands can be included on the QD. Here a cell-penetrating peptide has been co-grafted in a one-pot reaction to afford a cell-permeable multimodal multimeric MRI contrast agent that reports cellular localization by fluorescence and provides high relaxivity and increased tissue retention with respect to commercial contrast agents.

KEYWORDS: gadolinium · lanthanide complexes · imaging agents · quantum dots · fluorescence · magnetic resonance imaging

Functionalized nanoparticles have become key players for enhancing contrast of images in medical diagnostics and are essential in molecular imaging. Magnetic resonance imaging (MRI) is a powerful, noninvasive diagnostic tool with impressive anatomic resolution and tissue penetration, but applications are limited by its low sensitivity and lack of cell specificity. MRI contrast agents (CAs), primarily gadolinium Gd^{III} complexes, are used to enhance the image contrast. This enhancement is the result of the increase of the water proton relaxation rate, $1/T_1$, induced by the neighboring paramagnetic Gd^{III} ions. The efficiency of current commercial contrast agents, usually expressed in terms of their relaxivity r_1 (mM^{-1} s^{-1}), that is, the increase of $1/T_1$ per mM of added Gd^{III} complexes, is too low for the detection of events at the molecular scale. Moreover, commercial CAs are limited to extracellular applications. A possible approach for increasing MRI sensitivity is the use of multimeric CAs in which a large number of small Gd^{III} chelates are bound to a nanosized carrier allowing for the accumulation of paramagnetic Gd^{III} ions at the site of interest.[1−5]

Another approach consists in combining MRI with a different high-sensitivity imaging modality[6−8] such as fluorescence.[9−13] The accuracy of the analysis can be improved by a combined tissue study by optical microscopy and by MRI, which requires creating a multimodal reporter.[14] The majority of dual (MRI/optical) probes are MRI contrast agents coupled to organic dyes. More recently, dual probes have been identified where the optical reporter is a transition metal, a Ln^{III} complex, or a quantum dot.[10,11,14−16] Quantum dots (QDs) are highly luminescent, photostable semiconductor nanoparticles of size-controlled emission. They are very attractive for use in diagnostic, molecular, and cellular imaging due to their optical properties and their increased photostability as compared to organic dyes.[17−24] Luminescent lanthanide complexes, on the other hand, are characterized by large Stokes shifts and long-lived luminescence, which render them very attractive for applications in cellular imaging.[25−32] Bimodal probes can be obtained simply by mixing luminescent Ln^{III} and Gd^{III} ions complexed by the same ligand due to chemical equivalence (leading to similar biodistribution) of lanthanide complexes.[16,33,34] We have previously shown that the pyridinecarboxylate-based *bpatcn* (H_3bpatcn = 1-(carboxymethyl)-4,7-bis[(6-carboxypyridin-2-yl)methyl]-1,4,7-triazacyclononane) ligand can be used to prepare both a Tb^{III} complex with high luminescence quantum yield and a Gd^{III} complex with favorable relaxivity for MRI application.[35] Dual reporters have been demonstrated to be highly valuable in the multimodal imaging[36] studies of animals,

* Address correspondence to marinella.mazzanti@cea.fr.

Received for review July 27, 2011 and accepted September 3, 2011.

Published online September 03, 2011 10.1021/nn202839w

allowing the combination of preoperative and intraoperative visualization of tumors,[37] co-validation of CA distribution,[38] and combined tracking of transplanted stem cells.[39] A challenge in the development of MRI CAs for investigating biochemical processes and cellular events is the efficient delivery of agents across cellular membranes. For instance, the monitoring of cell fate and migration *in vivo* will be essential to the development of cell-based therapies. While the development of MRI/optical imaging agents has significantly increased in the past few years, there are only few examples of high Gd^{III} payload dual agents capable of penetrating cells.[9,11,40] QDs provide convenient scaffolds in the development and applications[41−43] of bimodal multimeric Gd-based CAs for molecular MRI.[11,13,14,44] Notably, multiple ligands can be simultaneously attached to the QD surface to promote cell penetration and/or specific targeting. Applications of Gd-chelate-functionalized QDs in molecular imaging have been reported by the groups of Mulder and Backes.[41−43,45] In the reported systems the gadolinium chelates were grafted through an "indirect" method involving the incorporation into a lipid coating or biotin−streptavidin interactions. Moreover, all the reported systems are based on established CdSe/ZnS QDs, whose applications are limited due to the intrinsic toxicity of cadmium.

Here we report a new MRI/optical probe based on nontoxic InP/ZnS QDs, which shows high relaxivity of 900 mM^{-1} s^{-1} at 35 MHz (0.81 T) and 298 K, obtained by the direct covalent attachment of around 80 Gd(bpatcn) complexes to the nanocrystal surface, giving a relaxivity of 13 mM^{-1} s^{-1} per Gd(bpatcn). The versatile synthetic strategy used herein allows the introduction of additional modalities on the QDs. In particular, the simultaneous grafting of the cell-penetrating peptide maurocalcine and of up to 40 gadolinium chelates affords a cell-permeable multimodal multimeric MRI CA. This multimodal agent reports cellular localization by fluorescence and provides bright MRI signal and increased tissue retention with respect to commercial contrast agents. We also demonstrate the covalent attachment of the chemically equivalent visible-emitting Tb- and Eu(bptacn) complexes, which provide a good analytical tool to monitor the grafting process and could be used in the development of different types of Ln-Gd-QD multimodal reporters including Ln-based and QD-based optical modalities.

RESULTS AND DISCUSSION

The previously reported [Ln(bpatcn)] complexes[35] were functionalized for grafting on InP/ZnS QDs according to Scheme 1 and Scheme S1. Complex Ln.1 is an amine-appended derivative of the [Ln(bpatcn)] complexes; Gd.1 has a r_1 of 4.12 mM^{-1} s^{-1} at 200 MHz (4.6T, 298 K), which is comparable to the previously reported bpatcn analogues[16] and commercial CAs.[46,47] Ligand L1 was prepared from 1,4,7-triazacyclononane-1,4-dibis(methylene)dipicolinic acid and 6-aminohexanoic acid in 62% yield through a multistep synthesis described in the Supporting Information. The amine functionality brings versatility, allowing for further modification. Notably, preliminary studies show that L1 can be directly conjugated through peptide chemistry coupling to different biomolecules such as peptides or oligonucleotides. In this work lipoic acid was successfully reacted with complex Ln.1 to afford the Ln.2 dithiol derivatives in 60% yield. The dithiol linker was chosen to ensure strong binding of the Ln chelates to the outer ZnS shell of the QDs.

InP/ZnS QDs are prepared in octadecene using phosphine gas as the phosphorus precursor and capped with a ZnS shell using a method we reported earlier.[48] Prior to the grafting of the water-soluble CA, a phase transfer reaction is performed using penicillamine at pH 9 in a 1:1 mixture of water and chloroform (reaction time 2 h, transfer yield 60%).[49] The InP/ZnS QDs capped with penicillamine (QD.Pen) provide a versatile platform for grafting of lanthanide chelates and/or other bioprobes.

The dithiol-functionalized lanthanide chelates are reacted overnight in a shaker with the QD.Pen in aqueous media at pH 9 and 20 °C in the presence of the reducing agent tris(carboxyethyl)phosphine (TCEP) to cleave the disulfide bond. This process results in the grafting of 75−80 lanthanide chelates on a single InP/ZnS QD in a 40% yield. The hydrodynamic diameters measured using dynamic light scattering (Table S1) showed an increase from 6.9 nm for the QD.Pen to 8.6−9.2 nm for the lanthanide complex functionalized QDs. This increase of around 2 nm is consistent with the successful coverage of the QD surface by Gd chelates. The strongest indication of successful grafting is the NMRD profile shown in Figure 1. Both Gd.1 and Gd.2 show a classical profile for monoaqua chelates. The Gd.2.QD system, with its larger molecular weight, shows a very different profile, with an increase in r_1 from 3 to 35 MHz (0.07−0.81 T, 298 K) of 10 to 13 mM^{-1} s^{-1}. The NMRD profile provides unambiguous evidence of efficient grafting and shows that the optimum relaxivity for Gd.2.QD is at 30 MHz (0.7 T, 298 K) with r_1 = 13 mM^{-1} s^{-1}. This significant increase in r_1 with respect to the nongrafted chelate is consistent with a slower rotation of the grafted complex due to its larger size. Increasing the molecular weight of Gd complexes by macromolecule and protein binding is an effective way to increase the relaxivity of small Gd chelates in the magnetic field range of 30−100 MHz (0.7−2.3 T, 298 K).[47] Magnetic susceptibility measurements and UV−visible spectroscopy showed the presence of 70−80 chelates grafted onto Gd.2.QD. As a result, the relaxivity per quantum dot reaches 900 mM^{-1} s^{-1}at 35 MHz (0.81 T, 298 K). As expected

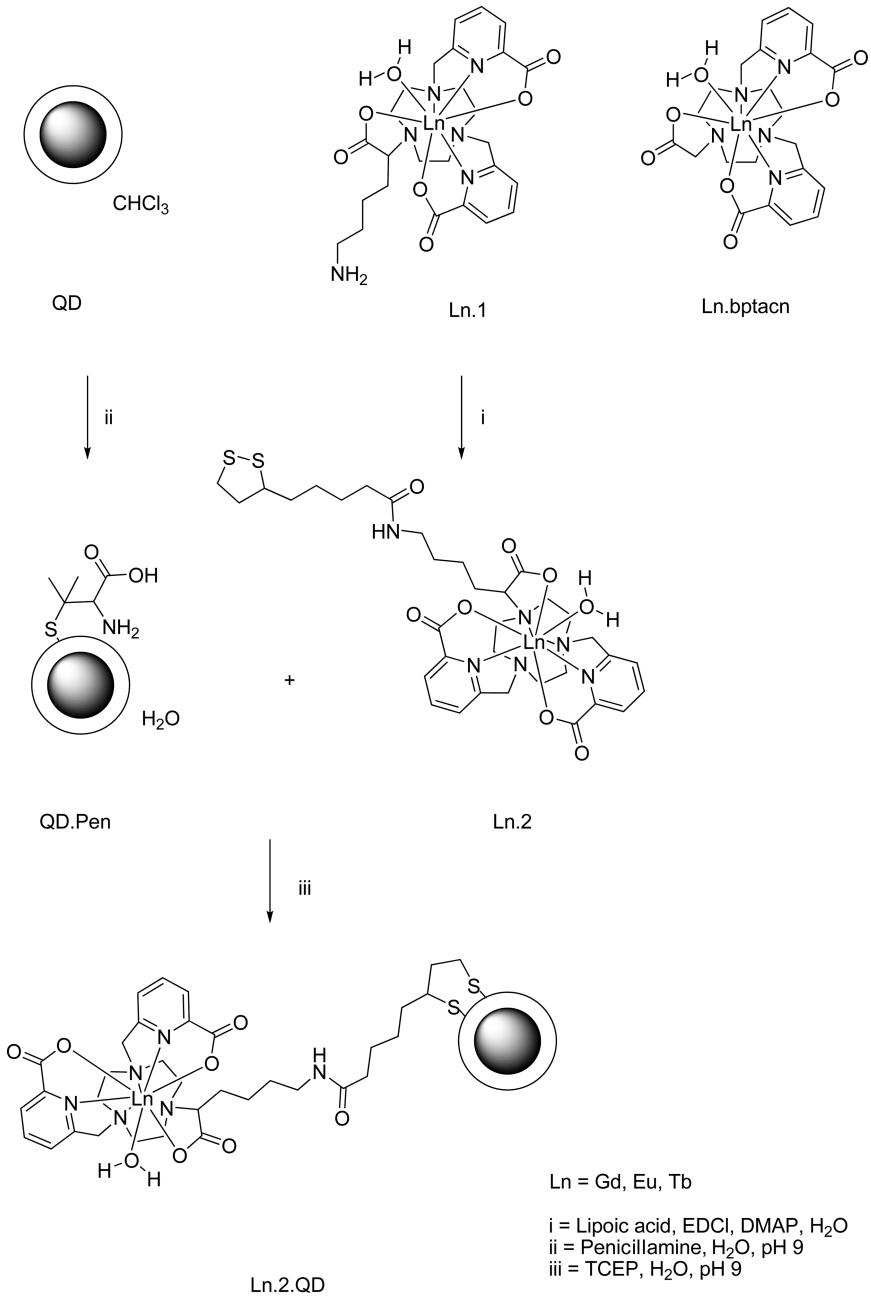

Scheme 1. Synthesis of Ln(III) QDs

from the theory of relaxivity, the slow rotation is not favorable at higher fields (200 MHz) and the relaxivity decreases, yielding a relaxivity per Gd chelate of 4.19 mM^{-1} s^{-1}. However, the relaxivity per quantum dot is still around 200 mM^{-1} s^{-1}, thus providing a very bright contrast agent compared to smaller chelates and commercial agents ($r_1 \sim 4$ mM^{-1} s^{-1}) (Figure S2).

In order to assess the full potential of Ln.2.QD systems as multimodal (optical/optical and optical/magnetic) contrast agents, we have investigated their photophysical properties. The water-dispersible penicillamine-capped InP/ZnS QDs show a fluorescence quantum yield (QY) of 8.5% in water. A significant decrease in QY (QY in chloroform: 20%) after phase transfer *via* surface ligand exchange is generally observed in the literature.[22] The lack of difference in the emission spectra of QD.Pen and Gd.2.QD (Figure S3) suggests that grafting of the complex does not affect the luminescence of the QDs, resulting in a magnetic and optical dual-mode imaging probe. The InP/ZnS photoluminescence peak is located at 620 nm, and the QY measured at 480 nm for Gd.2.QD in water (6.1%) is comparable to the value of QD-pen (8.5%). Since the picolinate ligand can efficiently sensitize terbium and europium (Figure S4), the grafting of chelates containing these visible-emitting lanthanide ions results in a dual-mode optical probe with emission from both the QD (nanosecond time scale) and the Tb or Eu ions

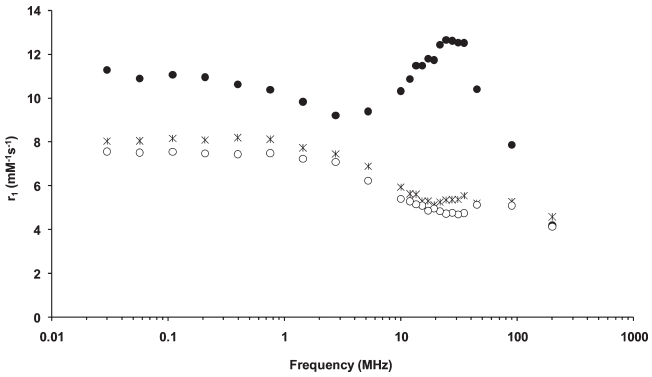

Figure 1. NMRD profile for Gd.1 (hollow circles), Gd.2 (crosses), and Gd.2.QD (full circles), at pH 7.4, 298 K.

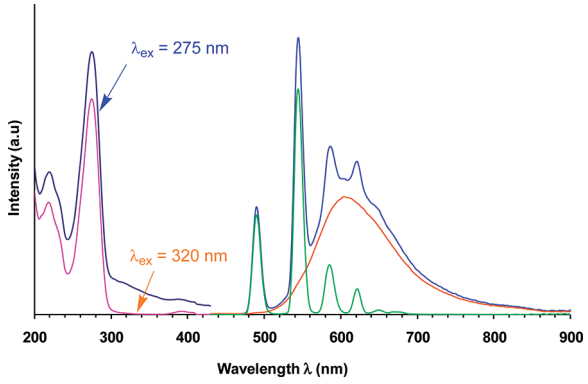

Figure 2. Luminescence of Tb.2.QD. (Left) Excitation spectra with λ_{em} = 546 nm (dark blue: 0 ms and pink: 0.05 ms delay, respectively). (Right) Emission spectra with λ_{ex} = 275 nm (blue: 0 ms and green: 0.05 ms delay, respectively) and 320 nm (orange: 0 ms delay).

(millisecond time scale). Energy transfer from Tb to QDs has been reported by Charbonniere for QDs grafted with Tb chelates through a streptavidine−biotine interaction.[20] In order to obtain dual-color systems, we have chosen QDs with emission matching the emission of the Eu and Tb complexes so that the energy transfer between the emitting centers is prevented. This strategy was successful, as no energy transfer was observed between the Tb or Eu and the QDs in our systems due the small energy gap between their emitting levels. Figure 2 shows the excitation and emission spectra of Tb.2.QD. The excitation spectrum of Tb.2.QD shows a large peak at 275 nm, corresponding to the picolinate ligand absorption, while the excitation corresponding to the QDs extends over the range 200−500 nm. Emission from one or the other of the two emitters or from both can be selectively turned on by a suitable choice of acquisition conditions. Notably, the excitation of Tb.2.QD at 275 nm with 0 ms delay yields dual emission from the QDs and Tb ions at 620 and 546 nm. When a 0.05 ms delay is applied, only the emission from the TbIII ions is observed due to their longer luminescence lifetime with respect to the QDs. Conversely, when Tb.2.QD is excited at 320 nm with 0 ms delay, only emission from the QDs is observed. This provides a dual luminescent probe, which has two defined emission wavelengths on two different time scales, the millisecond and the nanosecond scale. Similar results were obtained for Eu.2.QD (Figure S5).

The direct grafting of the Gd chelate on the QDs provides a bimodal architecture with high relaxivity and bright luminescence in water. The versatile synthetic method can be adapted to introduce on the QD one or several additional functionalities such as targeting and bioactive moieties or cell-penetrating ligands. Cell penetration is crucial for the use of CAs in the monitoring of biological events such as enzyme activity or pH and temperature changes or in the tracking of stems cells, but only few examples of cell-penetrating CAs have been reported. The peptide maurocalcine (MCa) coupled to commercial QDs has shown a great potential for cell penetration in *in vivo* imaging of macrophages as an indicator of atherosclerosis.[50] Therefore, we have used MCa as a cell-penetrating ligand for a further functionalization of our bimodal platform.

We conjugated reproducibly both Gd.2 and the cell-penetrating peptide maurocalcine in its disulfideless version[51] through an additional N-terminal cysteine residue onto the penicillamine-capped InP/ZnS QDs in a one-step synthesis using a QD:Gd.2:TCEP:MCa ratio of

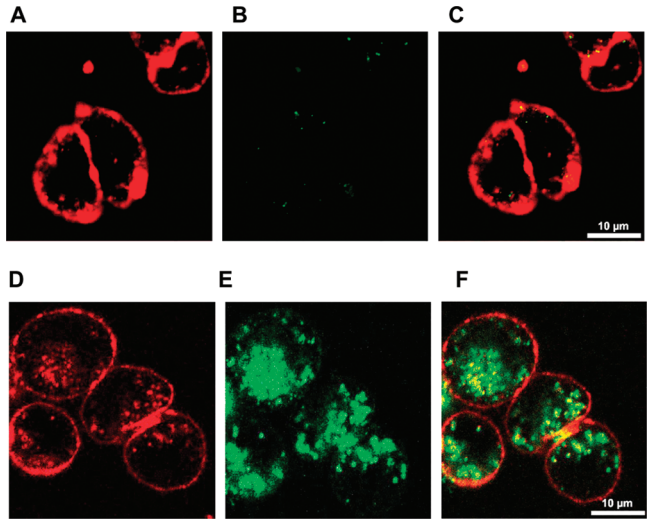

Figure 3. Confocal microscope images (false colors) of two batches of Chinese hamster ovarian cells (CHO). Batch 1: (A) stained with concanavalin A rhodamine (red); (B) incubation with Gd.2.QD (green) for 2 h followed by washing, (C) merge of A and B. Batch 2: (D) CHO cells as in A; (E) incubation with Gd.2.QD.MCa for 2 h followed by washing (green), (F) merge of D and E.

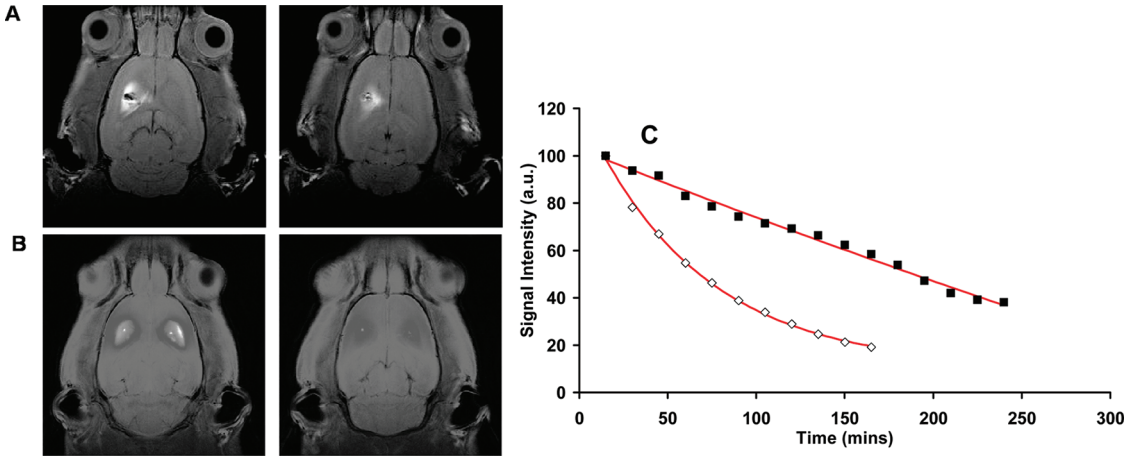

Figure 4. T_1-weighted MRI images of rat brain at 7 T (1 mM, 10 μL). (A) Gd.2.QD.MCa at 15 min and 4 h. (B) Dotarem at 15 min and 4 h. (C) Signal intensity *vs* time; Dotarem (◇) and Gd.2.QD.MCa (■).

1:200:9000:5. TCEP was used at high concentration to cleave the disulfide bridge of Gd.2 and to prevent the formation of undesired disulfide bridges. Magnetic susceptibility measurements[52] and UV−visible spectroscopy showed the presence of 30 to 40 Gd chelates on the MCa QDs.

In order to probe the cell-penetrating ability of this Gd.2.QD MCa dual probe, confocal microscopy images were recorded after incubation of the probe with Chinese hamster ovary (CHO) cells (Figure 3). They clearly show that the MCa-conjugated Gd.2.QDs accumulate within CHO cells during the 2 h incubation time, while no cell penetration is observed in the absence of MCa. Staining appeared as punctuate dots, suggesting that these MCa-functionalized QDs accumulate mostly in endosomes probably through an endocytosis-mediated uptake mechanism. The used resolution scale does not allow for the determination of the specific localization of Gd.2.QD.MCa. Some diffuse staining was also evident, suggesting that direct membrane translocation should not be excluded as one of the possible entry mechanisms. These data are coherent with earlier observations.[53] Importantly, similar experiments conducted with Gd.2.QD did not lead to intracellular accumulation of QD (Figure 3C), confirming that MCa was properly conjugated to Gd.2.QD and demonstrating that MCa is solely responsible for cell penetration of the complex.

The Gd.2Qd.MCa system provides a new, high-relaxivity bimodal probe that can penetrate cells. The cell permeability should lead to an increased retention of this contrast agent in brain tissue with respect to commercial CAs such as Dotarem ([Gd(DOTA)$^-$]). We therefore set out to compare whether Gd.2.QD.MCa provides a competitive advantage over Dotarem with regard to the retention time of the CA within the brain tissue.

To investigate this issue, 10 μL of 1 mM Dotarem or Gd.2.QD.MCa was injected directly into the striatum of 7-week-old rats (Figure 4). Both CAs led to a distinct signal within the injected striatum 15 min after injection. After 4 h, the Dotarem signal almost disappeared, whereas distinct signal intensity was still measurable for Gd.2.QD.MCa (Figure 4A).

Data analysis of the signal intensity over time illustrates that Dotarem concentration decreases rapidly in the striatum, whereas the Gd.2.QD.MCa concentration decrease is significantly slower over the 4 h period (Figure 4C). These data indicate a slower clearance of the Gd.2.QD.MCa with respect to Dotarem, which we attribute to a significant increase in tissue retention. While MCa is probably contributing to some extent to the improved duration of the MRI signal at the injection point, the size of the agents is an important factor limiting the lateral tissue diffusion of the compound.

CONCLUSIONS

Herein we have synthesized a new bimodal MRI/optical probe through direct grafting of gadolinium chelates on fluorescent InP/ZnS QDs. The high payload of gadolinium (up to 80 chelates) results in a high relaxivity of the nanosized contrast agent (900 mM^{-1} s^{-1}, 13 mM^{-1} s^{-1} per Gd ion at 35 MHz (0.81 T, 298 K), 200 mM^{-1} s^{-1}, 4.19 mM^{-1} s^{-1} per Gd ion at 200 MHz (4.6 T 298 K)), while the bright luminescence of the QDs is preserved. Chelates containing visible-emitting lanthanide ions have also been grafted on the QDs, and the absence of energy transfer between lanthanide ions and QDs results in a dual-mode optical probe with emission from the QDs and the Tb or Eu ions on different time scales (nanoseconds for the QDs, milliseconds for the rare earth ions). The versatile synthetic strategy allows the simultaneous grafting of various probes on the QDs. Notably, the protocol could be easily extended to produce a trimodal probe, optical (Tb-chelate)/magnetic (Gd-chelate)/optical (QD), and will be the subject of future work. We have also shown, through the example of the cell-penetrating peptide MCa, that additional targeting ligands can be co-grafted in a one-pot reaction. A new cell-penetrating multimodal probe has been identified that shows bright luminescence, high relaxivity, and excellent tissue retention properties, allowing for longer MRI recording than with commercial CAS.

METHODS

General Procedures. NMR spectra were recorded on Bruker DPX200 500 MHz spectrometers using standard Bruker software. Chemical shifts are reported in ppm with solvent as internal reference. ESMS were recorded on a Thermo Scientific (LXQ) spectrometer. Electronic absorption spectra were recorded on a Varian Cary 50 probe UV/vis spectrometer.

Materials. Solvents and starting materials were obtained from Aldrich, Fluka, Acros, and Alfa. They were used without further purification unless otherwise stated. Solvents were dried over the appropriate drying agents when required. Water and H_2O refer to high-purity water with a resistivity value of 18 M$\Omega\cdot$cm, obtained from the "Millipore/Milli-Q" purification system. Lanthanide chloride salts were purchased from Aldrich. Dotarem was purchased from Guerbet SA (Aulnay-s-bois, France). The precise metal ion content was titrated by colorimetry in acetate buffer (pH = 4.5) using standardized H_2Na_2edta solution (Merck) and xylenol orange indicator.

Ligand and Complex Synthesis. L1 was prepared from 1,4,7-triazacyclononane-1,4-dibis(methylene)dipicolinic acid[35] and 6-aminohexanoic through a multistep synthesis. The lanthanide complexes were formed in water. Synthetic procedures are detailed in the Supporting Information.

Quantum Dot Synthesis. The synthesis follows the protocol we reported earlier.[48] Briefly, the indium precursor (1 equiv of indium myristate in 1-octadecene) was reacted under an Ar atmosphere with *in situ* generated PH_3 gas at 250 °C for 60 min to form the core InP QDs. For growth of the ZnS shell, 10 equiv of zinc stearate was added into the dispersion of the InP NCs and heated for 4 h to 280 °C to form a Zn^{2+}-rich surface before injecting slowly 2.5 equiv of zinc ethylxanthate at 210 °C during 30 min.

Synthesis of Penicillamine-Capped QDs (QD-pen). Thorough purification of the initial QDs assuring the removal of excess hydrophobic ligands is crucial for the successful phase transfer. Five milliliters of the QDs in organic solvent was mixed with anhydrous ethanol (1:3) and centrifuged at 10 000 rpm (rotations per minute) for 6 min. The clear solution of supernatant was discarded, and the precipitate was redispersed in 15 mL of a 1:3 chloroform/ethanol mixture and centrifuged again. The precipitate was dispersed in a minimum amount of chloroform. The concentration was estimated from the first excitonic peak in the UV–vis spectrum.[23] A 0.2 M solution of penicillamine in degassed Milli-Q water (1 mL) with pH adjusted at 9 with 0.5 M TMAH (tetramethylammonium hydroxide) was mixed with a ~5 μM dispersion of the QDs in chloroform (1.5 mL). The resulting biphasic mixture was stirred vigorously at 1400 rpm for 2 h to afford a fine aqueous suspension of QD-pen, which was separated from the organic layer (yield: 60%).

Synthesis of Gd.2.QD. Solutions of Gd.2 (0.25 mL, 2.1 $\times$ 10^{-3} M) and TCEP (0.046 mL, 0.5 M) in degassed water were added to the suspension of QD-pen (0.5 mL, 5.2 $\times$ 10^{-6} M) in degassed water, and the pH of the resulting suspension was adjusted to 9 with 0.5 M TMAH. The mixture was shaken at 800 rpm overnight at 20 °C. The resulting fine suspension was purified portionwise (200 μL) using PES 30K centrifuge filters at 1400 rpm for 60 s. The obtained nanoparticles were washed with 3 $\times$ 150 μL of degassed H_2O/PBS to remove any ungrafted complex. The nanoparticle portions were combined and concentrated to 100 μL, giving a fine orange suspension (yield 40%). This procedure was repeated several times. A gadolinium content in the range 70–80 complexes per QD was determined for independent syntheses by combined magnetic susceptibility measurements and UV–vis spectroscopy.

Synthesis of Gd.2QD.MCa. Solutions of Gd.2 (0.25 mL, 2.1 $\times$ 10^{-3} M), TCEP (0.046 mL, 0.5 M), and maurocalcine (MCa) (0.054 mL, 2.5 $\times$ 10^{-5} M) in degassed water were added to the suspension of QD-pen (0.5 mL, 5.2 $\times$ 10^{-6} M) in degassed water, and the pH of the resulting suspension was adjusted to 9. The mixture was shaken at 800 rpm overnight at 20 °C. The resulting fine suspension was purified portionwise (200 μL) using modified PES 30K centrifuge filters at 1400 rpm for 60 s. The obtained nanoparticles were washed with 3 $\times$ 150 μL of degassed H_2O/PBS to remove any ungrafted complex. The nanoparticle portions were combined and concentrated to 100 μL, giving a fine orange suspension. This procedure was

repeated several times. A gadolinium content in the range 30−40 complexes per QD was determined for independent synthesis by combined magnetic susceptibility measurements and UV−vis spectroscopy. The concentration of the samples before phase transfer and after grafting is estimated from the first excitonic peak in the UV−vis spectra using the empirical correlations between the excitonic peak, size, and molar extinction coefficient compiled in ref 23. The concentration of Gd(III) was checked by the chemical shift measurement of HOD induced by the magnetic susceptibility.[52]

Relaxivity Measurements. The Gd.1 and Gd.2 samples were prepared *in situ* by mixing the appropriate amounts of ligand and $GdCl_3 \cdot 6H_2O$ (99.99%; Aldrich) in H_2O followed by adjustment of the pH with NaOH aqueous solution (pH = 7.4). The pH of the Gd2.QD suspension was adjusted for relaxivity measurements at 7.4. The resulting suspension was placed in a 1.7 mm diameter capillary, which was sealed. The absence of free gadolinium was checked in all samples by the xylenol orange test.[54] The NMRD profiles were measured at 298 K in the range 0.1 and 35 Mz, by using a Spinmaster FFC (fast field cycling) NMR relaxometer (Stelar, Italy). The $1/T_1$ measurement was performed on a Bruker Avance 200 spectrometer (200 MHz). The $1/T_1$ measurements at 45 MHz (1.06 T) and 298 K were performed on a BrukerMinispec "mqvar" ND2318. At higher magnetic fields relaxation measurements were performed on conventional high-resolution NMR spectrometers.

Luminescence Spectroscopy. Luminescence data were recorded using a Perkin-Elmer LS50B luminescence spectrometer (using FLWINLAB for Windows v2.2) and a a modular Fluorolog FL3-22 spectrometer from Horiba-Jobin Yvon-Spex. Samples were held in a 10 × 10 nm or 10 × 2 nm quartz Hellma cuvette, and a cutoff filter (450 nm) was used to avoid second-order diffraction effects.

Quantum Yield Measurements. The excitation source was a 450 W Xe arc lamp, and all spectra were corrected for detection and optical spectral response (instrumental functions) of the FL3-22 spectrofluorimeter. It is equipped with a double grating excitation monochromator and a iHR320 imaging spectrometer coupled to a R928P Hamamatsu photomultiplier for visible measurement. The quantum yields were determined at room temperature through an absolute method[55] using a home-modified integrating sphere coupled to the modular Fluorolog FL 3-22 spectrofluorimeter. The values reported are the average of three independent determinations for each sample. The absolute quantum yield was calculated using the following expression:

$$\Phi = \frac{E_c}{L_a - L_c} = \frac{E_c}{L_a \alpha} \text{ and } \alpha = \frac{L_a - L_c}{L_a}$$

where E_c is the emission spectra in the emission range of the sample (ex: if the emission maximum is 620 nm, the range of this spectrum will be from 450 to 750 nm), L_c is the emission spectra of the excitation wavelength of the sample, and L_a is the emission spectra of the excitation wavelength of the reference (quartz capillary tube 4 mm in diameter filled with the solvent used).

Lifetime Measurements and Time-Gated Experiments. Time-gated experiments were recorded using a 0.05 ms delay to remove luminescence from the QD. Excited-state lifetime measurements were made on a Perkin-Elmer LS50B luminescence spectrometer (using FLWINLAB for Windows). Lifetimes were measured by direct excitation (275 nm) of the sample with a short 40 ms pulse of light (500 pulses per point) followed by monitoring the integrated intensity of light (617 nm for Eu and 546 nm for Tb) emitted during a fixed gate time of 0.1 ms, at a delay time later. Delay times were set at 0.1 ms intervals, covering 4 or more lifetimes. Excitation and emission slits were set to 5:5 nm bandpass, respectively. The obtained decay curves were fitted to a simple monoexponential first-order decay curve using Microsoft Excel. *q*-Values were calculated using the following equations:[56]

$$q = 1.2[kH_2O - kD_2O - 0.25] \text{ forEu}$$

$$q = 5[kH_2O - kD_2O - 0.06] \text{ forTb}$$

DLS Measurements. The hydrodynamic diameter of the water-soluble NCs dispersed in water was measured by dynamic light scattering (DLS), using a Malvern Zeta Sizer (NanoZS). The samples have been thoroughly purified with centrifugal filters from VWR (MWCO 30k) and dispersed in Milli-Q water (18 mΩ·cm) prior to the measurements. Given the sensitivity of the instrument, multiple runs (>3) were performed to avoid erroneous results. The spectra have been corrected by the instrument software for viscosity (0.882 mPa·s at 25 °C), absorption (at 532 nm), solvent (water) refractive index (1.33), and material (InP) refractive index (3.1). The data are collected in automatic mode and expressed in number %.

TEM Image. TEM images of Gd.2.QD were taken with a JEOL 4000EX microscope operated at 400 kV. The samples were prepared by evaporating a drop of the colloidal solution on a copper grid supporting a thin carbon film.

Biological Tests. *CHO Cell Culture.* Chinese hamster ovary (CHO) cell line (from ATCC) was maintained at 37 °C in 5% CO_2 in F-12K nutrient medium (InVitrogen) supplemented with 10% (v/v) heat-inactivated fetal bovine serum (InVitrogen) and 10 000 units/mL streptomycine and penicillin (InVitrogen).

Confocal Microscopy. Live CHO cells were incubated for 2 h with 10 μM Gd.QD or Gd.QD-MCa in F-12K cell culture medium without serum. Immediately after a two-time washing procedure with F-12K medium, the cell plasma membrane was stained with 5 μg/mL rhodamin-conjugated concanavalin A for 5 min, and cells were then washed again with F-12K medium. Live cells were immediately analyzed by confocal laser scanning microscopy using a Zeiss LSM 710 (Gd.2.QD or Gd.2.QD.MCa) or a Zeiss AxioVert 200M. Rhodamine (580 nm) and QD (620 nm) were sequentially excited (at 488 nm for rhodamine and 561 nm for QD), and emission fluorescence was collected in *z*-confocal planes of 10−15 nm steps.

***In Vivo* MRI Studies.** All animal experiments were conducted in agreement with the "Principles of Laboratory Animal Care" (NIH publication no. 86-23, revised 1985). The guidelines of the French Ministry of Agriculture (87/848) and of the European Community (86/609/EEC) were also respected. The protocol was submitted for approval to the local neuroscience institute committee to minimize animal suffering and abusive use of animal numbers. OFA 7-week-old rats were anesthetized by 5% isoflurane inhalation in a mixture air/O_2 30% and maintained in anesthesia in 2% isoflurane. Rats were then injected with 10 μL of 1 mM Dotarem or Gd.2.QD.MCa (Dotarem or Gd.2 concentrationwise) in the striatum using a stereotaxic frame (coordinates: 0 mm frontal, 3.5 mm lateral, and 5.5 mm in depth) and at a rate of 2 μL/min. T_1-weighted images (spin−echo, T_R/T_E = 300/27 ms) of rat brain were acquired 15 min after intrastriatal injection and after placing the rats in a 7 T magnet (Bruker BioSpec 70/20 USR AVIII; Preclinical MRI Facility of Grenoble). Sequences of 16 slices (slice thickness: 1 mm each) over a period of 15 min were taken. This sequence was repeated over a 4 h period, thus leading to the total acquisition of 16 sets of 16 slices. The temperature was maintained at 37 °C throughout the experiments.

Data Analyses of MRI Images. Two types of MRI image analyses were performed. In each case, the most intense average T_1 signal was selected from the set of 16 images at T = 15 min and kept for all other times. First, a region of interest (ROI) was drawn (10 pixels) close to the injection point (*x* mm of the injection point), and the average signal intensity calculated over the ROI minus the average intensity of the contra-lateral control area (zone with contrast agent). This type of analysis provides a hint of signal reduction with time. Second, the same type of analysis was conducted by drawing a similar sized ROI at a distance of *y* mm away from the injection point, close to the outer limit of the detectable contrast agent signal. This second type of analysis provides some information about the lateral diffusion process of the contrast agent. Images and image analyses for Gd.2.QD.MCa were compared to Dotarem data.

Acknowledgment. This research was carried out in the frame of the EC COST Action D-38 "Metal-Based Systems for Molecular Imaging Applications" and the European Molecular Imaging Laboratories (EMIL) network. We acknowledge financial support from the French Research Agency (PNANO-07-NANO-044) and from CEA Technologies pour la Santé "TIMO-MA2" and thank L. Plassais for help with synthetic chemistry.

Supporting Information Available: Description of the material, extensive figures, and expanded discussions are available free of charge *via* the Internet at http://pubs.acs.org.

REFERENCES AND NOTES

1. Manus, L. M.; Mastarone, D. J.; Waters, E. A.; Zhang, X. Q.; Schultz-Sikma, E. A.; MacRenaris, K. W.; Ho, D.; Meade, T. J. Gd(III)-Nanodiamond Conjugates for MRI Contrast Enhancement. *Nano Lett.* **2010**, *10*, 484–489.
2. Datta, A.; Hooker, J. M.; Botta, M.; Francis, M. B.; Aime, S.; Raymond, K. N. High Relaxivity Gadolinium Hydroxypyridonate-Viral Capsid Conjugates: Nanosized MRI Contrast Agents. *J. Am. Chem. Soc.* **2008**, *130*, 2546–2552.
3. Castelli, D. D.; Gianolio, E.; Crich, S. G.; Terreno, E.; Aime, S. Metal Containing Nanosized Systems for MR-Molecular Imaging Applications. *Coord. Chem. Rev.* **2008**, *252*, 2424–2443.
4. Moriggi, L.; Cannizzo, C.; Dumas, E.; Mayer, C. R.; Ulianov, A.; Helm, L. Gold Nanoparticles Functionalized with Gadolinium Chelates as High-Relaxivity MRI Contrast Agents. *J. Am. Chem. Soc.* **2009**, *131*, 10828–10829.
5. Hooker, J. M.; Datta, A.; Botta, M.; Raymond, K. N.; Francis, M. B. Magnetic Resonance Contrast Agents from Viral Capsid Shells: A Comparison of Exterior and Interior Cargo Strategies. *Nano Lett.* **2007**, *7*, 2207–2210.
6. Frullano, L.; Catana, C.; Benner, T.; Sherry, A. D.; Caravan, P. Bimodal MR-PET Agent for Quantitative pH Imaging. *Angew. Chem., Int. Ed.* **2010**, *49*, 2382–2384.
7. Choi, J. S.; Park, J. C.; Nah, H.; Woo, S.; Oh, J.; Kim, K. M.; Cheon, G. J.; Chang, Y.; Yoo, J.; Cheon, J. A Hybrid Nanoparticle Probe for Dual-Modality Positron Emission Tomography and Magnetic Resonance Imaging. *Angew. Chem., Int. Ed.* **2008**, *47*, 6259–6262.
8. Tsotsalas, M.; Busby, M.; Gianolio, E.; Aime, S.; De Cola, L. Functionalized Nanocontainers as Dual Magnetic and Optical Probes for Molecular Imaging Applications. *Chem. Mater.* **2008**, *20*, 5888–5893.
9. Song, Y.; Xu, X. Y.; MacRenaris, K. W.; Zhang, X. Q.; Mirkin, C. A.; Meade, T. J. Multimodal Gadolinium-Enriched DNA-Gold Nanoparticle Conjugates for Cellular Imaging. *Angew. Chem., Int. Ed.* **2009**, *48*, 9143–9147.
10. Tu, C. Q.; Ma, X. C.; Pantazis, P.; Kauzlarich, S. M.; Louie, A. Y. Paramagnetic, Silicon Quantum Dots for Magnetic Resonance and Two-Photon Imaging of Macrophages. *J. Am. Chem. Soc.* **2010**, *132*, 2016–2023.
11. Mulder, W. J. M.; Koole, R.; Brandwijk, R. J.; Storm, G.; Chin, P. T. K.; Strijkers, G. J.; Donega, C. D.; Nicolay, K.; Griffioen, A. W. Quantum Dots with a Paramagnetic Coating as a Bimodal Molecular Imaging Probe. *Nano Lett.* **2006**, *6*, 1–6.
12. Howes, P.; Green, M.; Bowers, A.; Parker, D.; Varma, G.; Kallumadil, M.; Hughes, M.; Warley, A.; Brain, A.; Botnar, R. Magnetic Conjugated Polymer Nanoparticles as Bimodal Imaging Agents. *J. Am. Chem. Soc.* **2010**, *132*, 9833–9842.
13. Yang, H. S.; Santra, S.; Walter, G. A.; Holloway, P. H. Gd-III-Functionalized Fluorescent Quantum Dots as Multimodal Imaging Probes. *Adv. Mater.* **2006**, *18*, 2890–2894.
14. Jennings, L. E.; Long, N. J. 'Two is Better than One'-Probes for Dual-Modality Molecular Imaging. *Chem. Commun* **2009**, 3511–3524.
15. Koullourou, T.; Natrajan, L. S.; Bhavsar, H.; Pope, S. J. A.; Feng, J. H.; Narvainen, J.; Shaw, R.; Scales, E.; Kauppinen, R.; Kenwright, A. M.; *et al.* Synthesis and Spectroscopic Properties of a Prototype Single Molecule Dual Imaging Agent Comprising a Heterobimetallic Rhenium-Gadolinium Complex. *J. Am. Chem. Soc.* **2008**, *130*, 2178–2179.
16. Crich, S. G.; Biancone, L.; Cantaluppi, V.; Esposito, D. D. G.; Russo, S.; Camussi, G.; Aime, S. Improved Route for the Visualization of Stem Cells Labeled with a Gd-/Eu-Chelate as Dual (MRI and Fluorescence) Agent. *Magn. Reson. Med.* **2004**, *51*, 938–944.
17. Michalet, X.; Pinaud, F. F.; Bentolila, L. A.; Tsay, J. M.; Doose, S.; Li, J. J.; Sundaresan, G.; Wu, A. M.; Gambhir, S. S.; Weiss, S. Quantum Dots for Live Cells, in Vivo Imaging, and Diagnostics. *Science* **2005**, *307*, 538–544.
18. Lee, J. H.; Lee, K.; Moon, S. H.; Lee, Y.; Park, T. G.; Cheon, J. All-in-One Target-Cell-Specific Magnetic Nanoparticles for Simultaneous Molecular Imaging and SiRNA Delivery. *Angew. Chem., Int. Ed.* **2009**, *48*, 4174–4179.
19. Geissler, D.; Charbonniere, L. J.; Ziessel, R. F.; Butlin, N. G.; Lohmannsroben, H. G.; Hildebrandt, N. Quantum Dot Biosensors for Ultrasensitive Multiplexed Diagnostics. *Angew. Chem., Int. Ed.* **2010**, *49*, 1396–1401.
20. Hildebrandt, N.; Charbonniere, L. J.; Beck, M.; Ziessel, R. F.; Lohmannsroben, H. G. Quantum Dots as Efficient Energy Acceptors in a Time-Resolved Fluoroimmunoassay. *Angew. Chem., Int. Ed.* **2005**, *44*, 7612–7615.
21. Hussain, S.; Won, N.; Nam, J.; Bang, J.; Chung, H.; Kim, S. One-Pot Fabrication of High-Quality InP/ZnS (Core/Shell) Quantum Dots and Their Application to Cellular Imaging. *Phys. Chem. Chem. Phys.* **2009**, *10*, 1466–1470.
22. Yong, K. T.; Ding, H.; Roy, I.; Law, W. C.; Bergey, E. J.; Maitra, A.; Prasad, P. N. Imaging Pancreatic Cancer Using Bioconjugated InP Quantum Dots. *ACS Nano* **2009**, *3*, 502–510.
23. Reiss, P.; Protiere, M.; Li, L. Core/Shell Semiconductor Nanocrystals. *Small* **2009**, *5*, 154–168.
24. Parak, W. J.; Pellegrino, T.; Plank, C. Labelling of Cells with Quantum Dots. *Nanotechnology* **2005**, *16*, R9–R25.
25. Frias, J. C.; Bobba, G.; Cann, M. J.; Hutchison, C. J.; Parker, D. Luminescent Nonacoordinate Cationic Lanthanide Complexes as Potential Cellular Imaging and Reactive Probes. *Org. Biomol. Chem.* **2003**, *1*, 905–907.
26. Botta, M.; Quici, S.; Pozzi, G.; Marzanni, G.; Pagliarin, R.; Barra, S.; Crich, S. G. NMR Relaxometric Study of New Gd-III Macrocyclic Complexes and Their Interaction with Human Serum Albumin. *Org. Biomol. Chem.* **2004**, *2*, 570–577.
27. New, E. J.; Parker, D.; Smith, D. G.; Walton, J. W. Development of Responsive Lanthanide Probes for Cellular Applications. *Curr. Opin. Chem. Biol.* **2010**, *14*, 238–246.
28. Bunzli, J. C. G. Lanthanide Luminescence for Biomedical Analyses and Imaging. *Chem. Rev.* **2010**, *110*, 2729–2755.
29. Song, Y.; Kohlmeir, E. K.; Meade, T. J. Synthesis of Multimeric MR Contrast Agents for Cellular Imaging. *J. Am. Chem. Soc.* **2008**, *130*, 6662–6663.
30. Bunzli, J. C. G. Lanthanide Luminescent Bioprobes (LLBs). *Chem. Lett.* **2009**, *38*, 104–109.
31. Deiters, E.; Song, B.; Chauvin, A. S.; Vandevyver, C. D. B.; Gumy, F.; Bunzli, J. C. G. Luminescent Bimetallic Lanthanide Bioprobes for Cellular Imaging with Excitation in the Visible-Light Range. *Chem.—Eur. J.* **2009**, *15*, 885–900.
32. New, E. J.; Congreve, A.; Parker, D. Definition of the Uptake Mechanism and Sub-Cellular Localisation Profile of Emissive Lanthanide Complexes as Cellular Optical Orobes. *Chem. Sci.* **2011**, *1*, 111–118.
33. Lowe, M. P.; Parker, D.; Reany, O.; Aime, S.; Botta, M.; Castellano, G.; Gianolio, E.; Pagliarin, R. pH-Dependent Modulation of Relaxivity and Luminescence in Macrocyclic Gadolinium and Europium Complexes Based on Reversible Intramolecular Sulfonamide Ligation. *J. Am. Chem. Soc.* **2001**, *123*, 7601–7609.
34. Picard, C.; Geum, N.; Nasso, I.; Mestre, B.; Tisnes, P.; Laurent, S.; Muller, R. N.; Vander Elst, L. A Dual Lanthanide Probe Suitable for Optical (Tb^{3+} Luminescence) and Magnetic Resonance Imaging (Gd^{3+} Relaxometry). *Bioorg. Med. Chem. Lett.* **2006**, *16*, 5309–5312.
35. Nonat, A.; Gateau, C.; Fries, P. H.; Mazzanti, M. Lanthanide Complexes of a Picolinate Ligand Derived from 1,4,7-Triazacyclononane with Potential Application in Magnetic Resonance Imaging and Time-Resolved Luminescence Imaging. *Chem.—Eur. J.* **2006**, *12*, 7133–7150.
36. Frullano, L.; Meade, T. J. Multimodal MRI Contrast Agents. *J. Biol. Inorg. Chem.* **2007**, *12*, 939–949.
37. Kircher, M. F.; Mahmood, U.; King, R. S.; Weissleder, R.; Josephson, L. A Multimodal Nanoparticle for Preoperative Magnetic Resonance Imaging and Intraoperative Optical Brain Tumor Delineation. *Cancer Res.* **2003**, *63*, 8122–8125.
38. Mulder, W. J. M.; Strijkers, G. J.; Habets, J. W.; Bleeker, E. J. W.; van der Schaft, D. W. J.; Storm, G.; Koning, G. A.; Griffioen, A. W.; Nicolay, K. MR Molecular Imaging and Fluorescence Microscopy for Identification of Activated

Tumor Endothelium Using a Bimodal Lipidic Nanoparticle. *Faseb J.* **2005**, *19*, 2008–2010.
39. Modo, M.; Cash, D.; Mellodew, K.; Williams, S. C. R.; Fraser, S. E.; Meade, T. J.; Price, J.; Hodges, H. Tracking Transplanted Stem Cell Migration Using Bifunctional, Contrast Agent-Enhanced, Magnetic Resonance Imaging. *Neuroimage* **2002**, *17*, 803–811.
40. Olson, E. S.; Jiang, T.; Aguilera, T. A.; Nguyen, Q. T.; Ellies, L. G.; Scadeng, M.; Tsien, R. Y. Activatable Cell Penetrating Peptides Linked to Nanoparticles as Dual Probes for in Vivo Fluorescence and MR Imaging of Proteases. *Proc. Natl. Acad. Sci. U. S. A.* **2010**, *107*, 4311–4316.
41. Oostendorp, M.; Douma, K.; Hackeng, T. M.; Post, M. J.; van Zandvoort, M.; Backes, W. H. Gadolinium-Labeled Quantum Dots for Molecular Magnetic Resonance Imaging: R-1 Versus R-2 Mapping. *Magn. Reson. Med.* **2010**, *64*, 291–298.
42. Ostendorp, M.; Douma, K.; Hackeng, T. M.; Dirksen, A.; Post, M. J.; van Zandvoort, M. A. M.; Backes, W. H. Quantitative Molecular Magnetic Resonance Imaging of Tumor Angiogenesis Using cNGR-Labeled Paramagnetic Quantum Dots. *Cancer Res.* **2008**, *68*, 7676–7683.
43. Mulder, W. J. M.; Strijkers, G. J.; Nicolay, K.; Griffioen, A. W. Quantum Dots for Multimodal Molecular Imaging of Angiogenesis. *Angiogenesis* **2009**, *13*, 131–134.
44. Prinzen, L.; Miserus, R.; Dirksen, A.; Hackeng, T. M.; Deckers, N.; Bitsch, N. J.; Megens, R. T. A.; Douma, K.; Heemskerk, J. W.; Kooi, M. E.; *et al*. Optical and Magnetic Resonance Imaging of Cell Death and Platelet Activation Using Annexin A5-Functionalized Quantum Dots. *Nano Lett.* **2007**, *7*, 93–100.
45. van Tilborg, G. A. F.; Vucic, E.; Strijkers, G. J.; Cormode, D. P.; Mani, V.; Skajaa, T.; Reutelingsperger, C. P. M.; Fayad, Z. A.; Mulder, W. J. M.; Nicolay, K. Annexin A5-Functionalized Bimodal Nanoparticles for MRI and Fluorescence Imaging of Atherosclerotic Plaques. *Bioconjugate Chem.* **2006**, *21*, 1794–1803.
46. Powell, H. D.; Ni Dhubhghaill, O. M. N.; Pubanz, D.; Helm, L.; Lebedev, Y. S.; Schlaepfer, W.; Merbach, A. E. Structural and Dynamic Parameters Obtained from 17O NMR, EPR NMRD Studies of Monomeric and Dimeric Gd(III) Complexes. *J. Am. Chem. Soc.* **1996**, *118*, 9333–9346.
47. Merbach, A. E.; Toth, E. *The Chemistry of Contrast Agents in Medical Magnetic Resonance Imaging*; Wiley: Chichester, 2001.
48. Li, L.; Protiere, M.; Reiss, P. Economic Synthesis of High Quality InP Nanocrystals Using Calcium Phosphide as the Phosphorus Precursor. *Chem. Mater.* **2008**, *20*, 2621–2623.
49. Tamang, S.; Beaune, G.; Poillot, C.; De Waard, M.; Texier-Nogues, I.; Reiss, P. Compact and Highly Stable Quantum Dots Through Optimized Aqueous Phase Transfer. *Proc. SPIE* **2011**, *7909*, 79091B.
50. Jayagopal, A.; Su, Y. R.; Blakemore, J. L.; Linton, M. F.; Fazio, S.; Haselton, F. R. Quantum Dot Mediated Imaging of Atherosclerosis. *Nanotechnology* **2009**, *20*, 165102.
51. Ram, N.; Weiss, N.; Texier-Nogues, I.; Aroui, S.; Andreotti, N.; Pirollet, F.; Ronjat, M.; Sabatier, J. M.; Darbon, H.; Jacquemond, V.; *et al*. Design of a Disulfide-Less, Pharmacologically Inert, and Chemically Competent Analog of Maurocalcine for the Efficient Transport of Impermeant Compounds into Cells. *J. Biol. Chem.* **2008**, *283*, 27048–27056.
52. Corsi, D. M.; Platas-Iglesias, C.; van Bekkum, H.; Peters, J. A. Determination of Paramagnetic Lanthanide(III) Concentrations from Bulk Magnetic Susceptibility Shifts in NMR Spectra. *Magn. Reson. Chem.* **2001**, *39*, 723–726.
53. Ram, N.; Texier-Nogues, I.; Pernet-Gallay, K.; Poillot, C.; Ronjat, M.; Andrieux, A.; Arnoult, C.; Daou, J.; De Waard, M. In vitro and In Vivo Intracellular Delivery of Quantum Dots by Maurocalcine. *IJBNN* **2011**, *2*, 12–32. Esteve, E.; Mabrouk, K.; Dupuis, A.; Smida-Rezgui, S.; Altafaj, X.; Grunwald, D.; Platel, J. C.; Andreotti, N.; Marty, I.; Sabatier, J. M. *et al.* Transduction of the Scorpion Toxin Maurocalcine into Cells - Evidence that the Toxin Crosses the Plasma Membrane. *J. Biol. Chem.* **2005**, *280*, 12833–12839.
54. Brunisholz, G.; Randin, M. Sur la Separation des Terres Rares a Laide de Lacide Ethylenediamine-Tetraacetique 0.9. Procede en Cycle pour le Fractionnement des Terres Yttriques. *Helv. Chim. Acta* **1959**, *42*, 1927–1938.
55. deMello, J. C.; Wittmann, H. F.; Friend, R. H. An Improved Experimental Determination of External Photoluminescence Quantum Efficiency. *Adv. Mater.* **1997**, *9*, 230–232.
56. Beeby, A.; Clarkson, I. M.; Dickins, R. S.; Faulkner, S.; Parker, D.; Royle, L.; de Sousa, A. S.; Williams, G. J. A.; Woods, M. Non Radiative Deactivation of the Excited States of Europium Terbium and Ytterbium Complexes by Proximate Energy Matched Oh, Nh, Ch Oscillators: An Improved Luminescence Method for Establishing Solution Hydration States. *J. Chem. Soc., Perkin Trans. 2* **1999**, 493–503.